Understanding and tuning sliding friction

Liefferink, R.W.

Publication date
2021

CHAPTER 3

Ploughing friction on wet sand

In this chapter, the friction for sliding a hemisphere over partially water-saturated granular materials is investigated as a function of the water volume fraction. We find that ploughing friction is the main sliding mechanism: The slider leaves a deep trace in the sand after its passage. In line with previous research and everyday experience, we find that the friction force varies nonmonotonically with the water volume fraction. The addition of a small amount of water makes the friction force sharply drop, whereas too much added water causes the friction force to increase again. We present a ploughing model that quantitatively reproduces the nonmonotonic variation of the friction force as a function of water volume fraction without adjustable parameters. In this model, the yield stress of the water-sand mixture controls the depth to which a hemispherical slider sinks into the sand and, consequently, also the force that is required to plough through the water-sand mixture.

3.1 Introduction

The mechanics of sliding over or digging in soil is crucial to many natural phenomena such as plant root growth [68–70], terradynamics [71,71] and antlion hunting strategies [72,73]. Industrially, very similar phenomena control processes in agriculture [74], the production of pharmaceuticals [75] or soil transport through pipes [76]: The importance of the manipulation of granular materials is difficult to overestimate since more than 10% of the world energy consumption is spent on it [77]. In all of the above phenomena and processes, the mechanics of granular materials is greatly impacted by the presence of small amounts of water.

When water is introduced to a granular system, liquid bridges form between neighbouring grains and bind them together, resulting in a cohesive material [50, 78–82]. The stiffness of a granular material, quantified, for instance, by the elastic shear modulus G', varies nonmonotonically with the addition of liquid [51]. The stiffness is optimal when small liquid bridges form between the grains, which results in attractive forces binding the granular material together. At higher water contents, the capillary bridges start to coalesce, thereby decreasing the shear modulus. This intricate interplay between mechanical strength and water content can be illustrated by building sandcastles with sand that has been wetted with a varying amount of water: The highest sandcastle is constructed by mixing the sand with some (but not too much) water [83].

Remarkably, sliding friction on water-sand mixtures follows very similar (nonmonotonic) behaviour in which the addition of a few percent of water can greatly reduce the friction while too much water makes the sand muddy and difficult to slide over [6]. In this chapter we present sphere-on-sand sliding experiments and show that the relation between the friction force and stiffness is fully described by a ploughing model that takes advantage of the simple sphere-on-flat geometry.

3.2 Experiments

In the sliding experiments, we use the custom-made tribometer (see Section 2.1.1 for more details) to horizontally slide a stainless steel hemisphere of radius $R = 52.5\,\mathrm{mm}$ over a water-sand mixture [Fig. 3.1(a)]. The normal force N is controlled by filling the hemisphere with dead weights. At a sliding speed of 4 mm/s over a total sliding distance of 130 mm the friction force F is monitored. Variation of the sliding speed

in the range from 0.1 mm/s to 13 mm/s does not lead to an appreciable change in friction force in this regime. All experiments are performed using polydisperse ($100 - 1000\ \mu$m grains) ISO 679 standard sand, which is first dried in an oven and cooled down to room temperature. Subsequently, the sand is thoroughly mixed with demineralised water and compacted by repeated tapping.

In addition to the forces, the final radius r of the track drawn in the water-sand mixture perpendicular to the movement is measured. This enables us to calculate the ploughing cross section A_P and the projected contact area A_c [Fig. 3.1(b-c)]. The penetration hardness, the contact pressure at yielding, can then be obtained from the contact area A_c: $P_\mathrm{h} = N/A_\mathrm{c}$. Note that, in contrast to the indentation experiments discussed in Section 2.2, the dynamic contact area while sliding is only based on the front part of the sphere: $A_\mathrm{c} = \frac{1}{2}\pi r^2$. Using varying dead weights, the normal force was varied from 2.5 N up to 16 N for each water-sand mixture and subsequently the

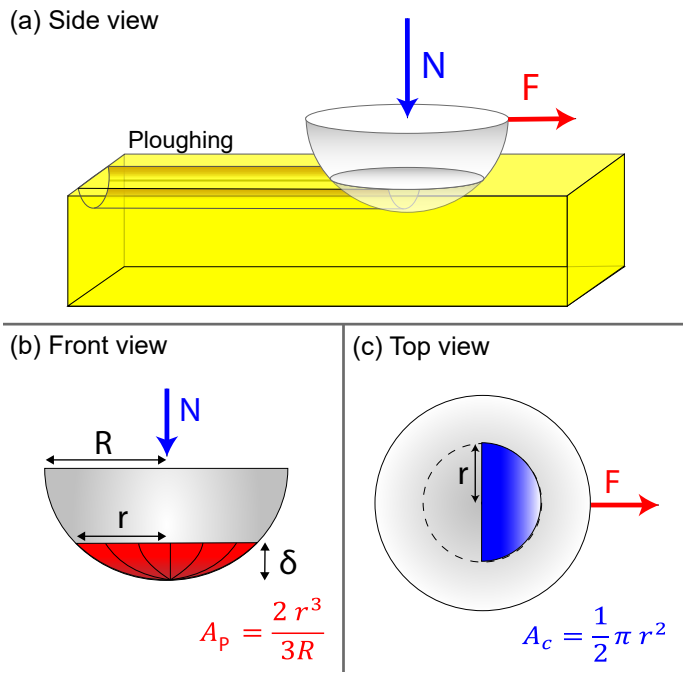

Figure 3.1: Schematic representation of the ploughing experiment. **a)** Side view: Normal (N) and frictional (F) forces which act on the sliding hemisphere. **b)** Front view: The hemisphere with radius R, where the ploughing cross section A_P (red) can be calculated using the track radius r. **c)** Top view: The hemisphere with the projected area of contact A_c (blue).

track radius is measured, and the average penetration hardness is calculated.

Furthermore, the ploughing cross section A_P can be calculated with the track radius r. The cross section can be written as $A_\mathrm{P} \approx \frac{4}{3} r\delta$ with the depth of penetration $\delta \approx \frac{r^2}{2R}$ if $\delta << R$. Consequently, the ploughing area is $A_\mathrm{P} = \frac{2r^3}{3R}$. Note that the assumption $\delta << R$ results in a relative error in A_P and μ [with Eq. (3.2)] of less than 4.5% for $r \leq 20$ mm ($\frac{r}{R} \leq 0.38$). However, for $r = 40$ mm, the relative error increases to 21%, which results in an underestimation of the friction coefficient for $\phi_\mathrm{w} = 0\%$ in Figure 3.2.

3.3 Results

3.3.1 Ploughing through wet sand

In agreement with earlier measurements [6], we find that the friction coefficient first decreases as more water is added to the sand, and then increases again (see Fig. 3.2). What mechanism drives this nonmonotonic variation of the friction force with water content? In each of the sliding experiments, the hemisphere creates a clear ploughing track, the width of which can be measured after the sliding stops. Interestingly, we find that the width of the ploughing track also varies nonmonotonically with the water volume fraction, just like the friction coefficient (Fig. 3.3): Sliding is more

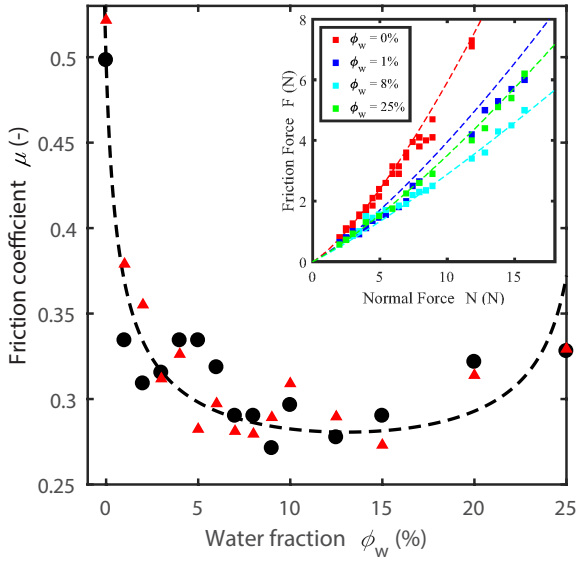

Figure 3.2: Evolution of the friction coefficient μ for the water volume fraction ϕ_w. The friction coefficient obtained from the measured friction force and fixed normal force ($N = 7.9$ N) in black circles display a nonmonotonic behaviour for increasing water fractions. With use of the ploughing model, the friction coefficient can be either modelled based on the ploughing track radius r [Eq. (3.2) in red triangles] or based on the penetration hardness P_h of the water-sand mixture [Eq. (3.3), dashed line]. The inset shows the friction force as function of the normal force for various water volume fraction experimentally (squares) and predicted by the ploughing model based on the penetration hardness P_h (dashed line).

difficult when the hemisphere sinks deeper into the sand.

The presence of a ploughing track indicates that during sliding, the water-sand mixture is plastically deformed in both the normal and tangential directions. To quantify the stresses involved in this plastic deformation we simply divide the external forces by the area on which they act. In the normal direction, the gravitational force that acts on the hemisphere is supported by the projected area of contact $A_c = \frac{1}{2}\pi r^2$ [see Fig. 3.1(c)] leading to an average contact pressure of $P_h = N/A_c$ which defines the penetration hardness of the water-sand mixture, P_h (Fig. 3.4). We find that the addition of some (but not too much) water has a dramatic effect on the penetration hardness of the compacted water-sand mixture: While dry sand can only support a stress of 3 kPa, ideally wetted sand supports up to 80 kPa of normal stress before showing a marked plastic deformation. When too much water is added to the sand, the mixture becomes muddy and the penetration hardness drops again to a value of 20 kPa at 25% water volume fraction.

The nonmonotonic behaviour of the penetration hardness is qualitatively similar

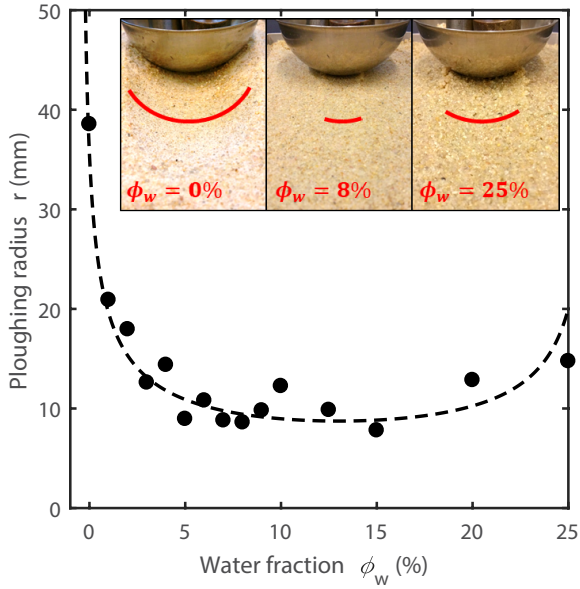

Figure 3.3: Ploughing radius r as a function of water volume fraction ϕ_w for a fixed normal force of $N = 7.9$ N. Like the friction coefficient, the ploughing track width (black circles) evolves nonmonotonically with the water content, also shown based on the ploughing model (dashed line, $r = \sqrt{\frac{N}{\frac{1}{2}\pi P_h(\phi_w)}}$). The inset shows images of the experiments for $\phi_w = 0$, 8 and 25% with red lines highlighting the ploughing tracks.

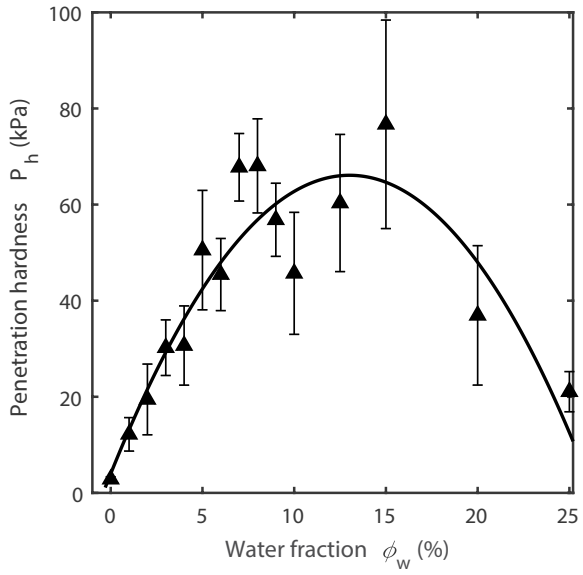

Figure 3.4: Penetration hardness P_h as a function of water volume fraction ϕ_w. The error bars represent the standard deviation. The solid line describes the data based on a first-order increase due to liquid bridge formation and an exponential decrease based on the coalescence of these liquid bridges.

to that of the elastic shear modulus. The physics behind the behaviour of the latter is fully (and quantitatively) understood: The initial increase when small amounts of water are added is due to the formation of more and more liquid bridges between neighbouring grains. The subsequent decrease at higher water content results from the filling up of the bridges: The smaller the liquid bridge, the higher the Laplace pressure holding two grains together and hence the stiffer the system; ultimately the coalescence of the liquid bridges at even higher water content leads to an even smaller modulus, as the Laplace pressure becomes very small [51]. The behaviour of the modulus can be roughly approximated by first a linear increase with increasing water content; for a fixed bridge volume the number of bridges scales linearly with the amount of fluid added [51]. For the decrease of the stiffness, the coalescence of the liquid bridges is the dominant effect; we can assume that this is a random (Poisson) process, so that an exponential decrease of the hardness should be observed for increasing water content. If we apply the same ideas to the penetration hardness, we get a very satisfactory description of the data, given by the solid line Figure 3.4.

3.3.2 The ploughing model

The penetration hardness then controls the depth to which the hemisphere penetrates the water-sand mixture. Therefore, if the load is varied, the contact area increases until the pressure again reaches the penetration hardness. Consequently, the ploughing track increases with increasing normal force, as is shown in Figure 3.5 for several water fractions. The dashed line represents the ploughing track radius based on the calculated average penetration hardness with $r(\phi_w, N) = \sqrt{\frac{N}{\frac{1}{2}\pi P_h(\phi_w)}}$. The ploughing motion of the hemisphere involves an analogous deformation in the tangential direction.

We now use a well-known method introduced for metal-on-metal ploughing [45,46] to calculate the ploughing force. Ploughing starts if the tangential pressure on the water-sand mixture exceeds its penetration hardness P_h; therefore, the ploughing force can be written in terms of the penetration hardness and the cross-sectional area

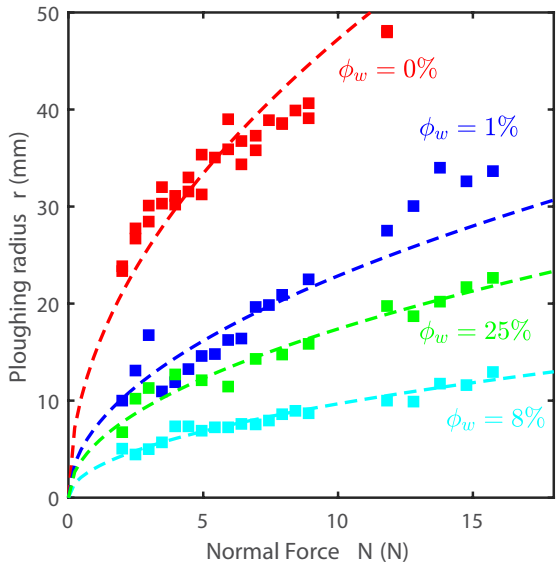

Figure 3.5: Ploughing radius r as a function of normal force N for various water volume fractions. The squares represent the experimental data and the dashed lines reflects the model ($r = \sqrt{\frac{N}{\frac{1}{2}\pi P_h(\phi_w)}}$) based on the penetration hardness. The radius increases with the normal force and has a minimum for $\phi_w = 8\%$. Note that the nonmonotonic behaviour of the track radius for increasing water content holds over the full domain of normal forces.

as $F_P = P_h A_P$ with $A_P = \frac{2r^3}{3R}$ [see Fig. 3.1(b)]. Subsequently, the friction coefficient is the ratio of the ploughing force to the normal force

$$\mu = \frac{P_h A_P}{N} + \mu_0 \,. \tag{3.1}$$

To account for the fact that even in the absence of ploughing a frictional force will resist the sliding, we introduce μ_0 as the surface friction contribution. Using the definition of the penetration hardness and Equation (3.1), the friction coefficient μ can now be expressed in terms of the ploughing track size as

$$\mu = \frac{4\, r(\phi_w, N)}{3\pi R} + \mu_0 \,. \tag{3.2}$$

Equation (3.2) indeed suggests that the deeper the hemisphere ploughs into the sand the larger the friction, as observed in Figures 3.2 and 3.3. Furthermore, from Equation (3.2) we can now calculate the friction coefficient using the imposed normal force N, the measured track width r and the surface friction contribution μ_0. Indeed, the calculated friction coefficient is in good agreement with the measured friction coefficient (black circles and red triangles in Figure 3.2).

Alternatively, the friction coefficient can be expressed in terms of the penetration hardness P_h, the imposed normal force N and the surface friction coefficient μ_0:

$$\mu = \frac{4\sqrt{2}}{3\pi^{3/2} R} \sqrt{\frac{N}{P_h(\phi_w)}} + \mu_0 \,. \tag{3.3}$$

In Figure 3.2 we plot this function (dashed line) using the relation between penetration hardness and water content obtained for normal forces ranging from 2.5 N to 16 N in Figure 3.4. Again, we find good agreement between the ploughing model and the experiment. Finally, Equation (3.3) explicitly predicts a super-linear increase of the friction force F as a function of the normal force: $F \sim N^{3/2} + \mu_0 N$. We indeed observe such behaviour for different water-sand mixtures (inset Fig. 3.2); also note that the nonmonotonic behaviour of the friction force for increasing water content is sustained over the full range of imposed normal forces probed here.

The only adjustable parameter in the ploughing model is the surface friction contribution, $\mu_0 = 0.21$, corresponding to the sliding friction between the hemisphere and the sand grains. When there is no permanent deformation of the water-sand packing, we expect the total friction to be equal to μ_0: $\mu = \mu_0$, corresponding to $R = 0$ in Equation (3.2). To obtain exactly this type of sliding motion, we now fix a collection of sand grains to a plate using glue. The hemisphere is then pulled over these immobilised sand grains using normal forces ranging from 2.5 N up to

16 N. The measured friction coefficient, $\mu_0 = 0.19 \pm 0.09$, is in good agreement with the value that was used to match the ploughing model to the experimental data in Figure 3.2: $\mu_0 = 0.21$.

3.4 Discussion

We have shown the influence of the hardness on the friction force when a hemisphere with an imposed normal force ploughs through a water-sand mixture. When the hardness of the granular material is high, the slider has a small indentation depth and a shallow ploughing track which, consequently, results in a low friction coefficient: high hardness is low friction. However, the ploughing model is not limited to load-controlled sphere-on-flat sliding experiments. In Figure 3.6 the influence

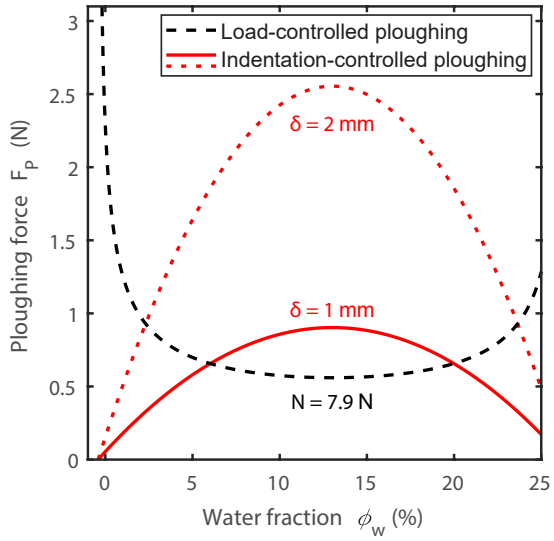

Figure 3.6: Ploughing force F_P as a function of water volume fraction ϕ_w. The black dashed line gives the load-controlled ploughing model [Eq. (3.3)] for sliding a hemisphere ($R = 52.5$ mm) at a load of $N = 7.9$ N over a water-sand mixture with a given hardness P_h (see Fig. 3.4). In the red continuous and dashed lines, the indentation-controlled ploughing model for a set indentation depth of, respectively, $\delta = 1$ mm and $\delta = 2$ mm. The indentation depth and the radius of the hemisphere ($R = 52.5$ mm) sets the ploughing area A_P which are 13.7 mm^2 and 38.6 mm^2 for, respectively, the red continuous and dashed lines.

of load- or indentation-controlled sliding is illustrated where the ploughing force F_P is plotted for increasing water volume fractions. The load-controlled ploughing force is shown in the dashed line for the experimentally set conditions ($N = 7.9$ N, $R = 52.5$ mm) where the red lines represent the indentation-imposed ploughing force for, respectively, $\delta = 1$ mm and $\delta = 2$ mm. For a set indentation the ploughing area A_P is constant and, subsequently, the ploughing force can be written as $F_P(\phi_w) = P_h(\phi_w)A_P$. Therefore, indentation-controlled sliding experiments, where the ploughing area is fixed, result in a ploughing force that is proportional to the hardness.

Here we quantify the penetration hardness based on the ploughing track and normal force when sliding tangentially. The penetration hardness of wetted granular materials can also be measured by performing indentation experiments as introduced in Chapter 2 and performed in Chapter 4 which results in qualitatively similar nonmonotonic behaviour of the penetration hardness as a function of the water content.

The influence of the large variation of the hardness with the water fraction is not restricted to pulling a sphere over wetted sand. For example, the impact cratering of a sphere in a granular material depends strongly on the water fraction. Marston et al. [84] present experimental results for the penetration of a solid sphere when released on a granular material. The minimum penetration depth of the object (corresponding to a zero-impact speed) and yield stress of the granular material reveal qualitatively similar nonmonotonic behaviour as a function of increasing water fractions compared to that found here for the width of the ploughing track and the penetration hardness. Furthermore, the hardness-controlled ploughing quantified here is not specific for granular materials as ploughing is a typical form of wear that is generally encountered when one of the two materials is much harder than the other. In metal-metal systems, the increase of friction with penetration depth is well known [45, 46]. Friction on ice for instance, depending on the conditions, can be dominated by ploughing. In Chapter 5 we measure the penetration hardness of ice and the sphere-on-ice sliding friction as a function of temperature and speed. Close to the melting point ploughing behaviour is observed; the slider penetrates the ice and leaves ploughing tracks on the ice surface. Our simple ploughing model also captures the evolution of sphere-on-ice friction.

3.5 Conclusion

We have presented sliding experiments of a hemisphere on wetted sand in which we imposed the normal force and measured the pulling force and the width of the ploughing track. For a given normal force, both the pulling force and the width of the ploughing track show a minimum for a water volume fraction of around 10%, where the measured penetration hardness of the water-sand mixture is maximal. This behaviour is fully consistent with the ploughing model in which the sphere-on-flat geometry is exploited to express the friction coefficient as a function of the normal force and penetration hardness (or ploughing track radius).